

pubs.acs.org/joc Article

New Design Strategy Toward NIR I Xanthene-Based Dyes

Ishanka Rajapaksha, Hao Chang, Yao Xiong, Seth Marder,* Steven R. Gwaltney,* and Colleen N. Scott*



Cite This: J. Org. Chem. 2020, 85, 12108-12116



ACCESS

III Metrics & More

Article Recommendations

SI Supporting Information

ABSTRACT: An effective design strategy with an efficient synthetic route to xanthene-based far-red to near-infrared dyes is reported. The dyes were prepared by the Suzuki cross-coupling of the electron-poor fluorescein ditriflate with the electron-rich boronic acid/ester-functionalized pyrrole (2C/3C) and indole (2D/3D) moieties. Upon treatment with trifluoroacetic acid, the closed nonfluorescent forms of the dyes (2C and 2D) ring-opened to their fluorescent forms (3C and 3D). The absorption maxima were 665 and 704 nm, while the emission maxima were 717 and 719 nm for 3C and 3D, respectively. The closed forms of the dyes were soluble in chloroform and acetonitrile. To test the efficacy of the dyes as probes, a turn-off fluoride ion probe was prepared from 3C, which consisted of a silyl ester receptor. The probe responded

Rhodamine B λ_{ab} , 540 nm λ_{cm} 565 nm

Rhodamine B λ_{ab} , 540 nm λ_{cm} 717 nm

strongly to low concentrations of fluoride, carbonate, and acetate ions, weakly to phosphate ions, but not to the other halogens. Moreover, the probe can detect the minimum concentration of F^- in water.

■ INTRODUCTION

Organic dyes that absorb light in the far-red to near-infrared I (NIR I) region (600–900 nm) are of interest because of their potential for use in applications such as NIR light-emitting diodes, solar cells, dye-sensitized solar cells (DSC), photodynamic therapy, and biological imaging. Metal-free organic dyes that are lightweight, inexpensive, and easily processed could be of particular interest. The classic classes of metal-free red to NIR I organic dyes include squaraines, cyanines,⁷ phthalocyanine and porphyrin,^{4c,8} BODIPY analogs,9 diketopyrrolopyrroles,10 and xanthene dyes.11 Among the many dye structures, the xanthene-based dye, rhodamine, and its derivatives are known for their excellent photophysical properties such as long absorption and emission wavelength, high fluorescence quantum yield, and large extinction coefficient and some have exhibited high photostability. 12 Rhodamine dyes can possess good water solubility with appropriate substitution. 13 In addition to their excellent photophysical properties, rhodamine dyes can undergo a molecular switching process between the closed, colorless spirocyclic structures to the opened and highly colored form upon stimulation by analytes (Figure 1).¹⁴ Hence, these dyes have been widely explored as colorimetric probes.

Rhodamine derivatives exhibit maximum absorption in the visible region with wavelengths around 400–600 nm. Extending the absorption and emission wavelengths of these dyes has been the focus of several research groups. In 2008, Fu et al. reported a long-wavelength silaanthracene derivative by replacing the bridged oxygen atom with silicon. The new probe had a 90 nm bathochromic shift in its absorption and

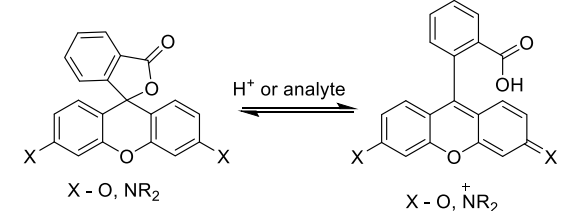


Figure 1. Molecular structure switching for the xanthene-based dyes fluorescein and rhodamine.

emission wavelength compared to rhodamine B. This innovative concept was further explored by Nagano and coworkers who replaced the bridged oxygen atom in rhodamine by the group 14 elements Si and Ge to prepare rhodamine derivatives in the far-red to NIR I region; the Sn derivative was not stable and could not be isolated. The Si-based rhodamine derivative had a maximum absorbance at 646 nm and emission at 660 nm, while the Ge based derivative showed absorption maxima 635 nm and emission maxima at 649 nm. A similar effect was seen for the Si-fluorescein derivative. The Furthermore, Yamaguchi et al. prepared highly photostable far-red to NIR I emissive rhodamine and fluorescein dyes by replacing the

Received: May 22, 2020 Published: August 24, 2020





Scheme 1. Synthesis of Derivatives of Rhodamine Dyes (3A-3D)

bridging O atom with a phosphine oxide moiety. 18ab The phospha-fluorescein dye showed absorption and emission maxima at 627 and 656 nm, respectively, while phospharhodamine dyes showed absorption and emission maxima around 712 and 740 nm. 18c Other examples of NIR I xanthene derivatives add an electron-withdrawing group at the 9th position or extend the π -conjugation system of the xanthene skeleton of rhodamine dye. The π -conjugation strategy produced NIR I dyes with absorption maxima at 688-728 nm and emission maxima at 721-763 nm with excellent photophysical properties. Unfortunately, all of these design strategies to produce far-red to NIR I xanthene-based dyes require lengthy synthetic steps for their preparation, which are not desirable for scale-up protocols. Subsequently, we designed far-red to NIR I xanthene-based dyes that can be prepared in good yields using efficient synthetic routes.

Our design strategy involves conjugating the electron-deficient xanthene core to the electron-rich pyrrole and indole rings at the C-2 position rather than the N-position. This approach leads to a decrease in the π - π * energy gap due to the extended π -conjugated system, resulting in a red shift in the absorption and emission maxima. We can prepare these dyes in two synthetic steps starting from the readily available fluorescein compound. Herein, we report on the efficient synthesis and photophysical properties of far-red to NIR I

xanthene-based dyes. Furthermore, the most promising dye was selected to test the response of our probe to an analyte. In this regard, we report the synthesis and analysis of a silylethyl ester xanthene derivative that functions as a fluoride ion turn-off probe.

■ RESULTS AND DISCUSSION

The syntheses of our new xanthene-based dyes began with fluorescein ditriflate (1), which was reported by Lavis and coworkers.²⁰ Additionally, the Lavis group performed the Buchwald/Hartwig cross-coupling reaction of 1 with pyrrole and indole to prepare analogs of rhodamine (Scheme 1, 2A and 2B). The optical properties were measured in a 1% v/v DMSO and it was determined that 2A showed no absorption between 300 and 800 nm, while the maximum absorption wavelength for 2B was 315 nm. Neither compound displayed fluorescence in the solution. Using Lavis' protocol, in two synthetic steps, we also prepared 2A and 2B and converted them to their highly colored ring-opened form (3A and 3B) by treatment with trifluoroacetic acid (TFA) in chloroform (CHCl₃) (Scheme 1). Alternatively, 3',6'-dibromofluoran²¹ can be prepared in one step from 3-bromophenol and phthalic anhydride and used in place of compound 1. Subsequent investigation of their photophysical properties reveals that the absorption and emission maxima of 3A (528 and 535 nm

respectively) are too low to be considered in the far-red to NIR (I) region; however, the absorption and emission maxima for 3B (623 and 709 nm, respectively) are in the far-red to NIR I region (Table 1, Figure 2A–D). Additionally, the Stokes shift

Table 1. Photophysical Properties of Probes 3A-3D in CHCl₃

probes	λ_{abs} (nm)	λ_{em} (nm)	Φ_{fl} (%)	$\Delta\lambda$ (nm)	$\varepsilon \; (\mathrm{M^{-1} \; cm^{-1}})$
3A	528	535		7	91 500
3B	623	709		86	38 400
3C	665	717	6	52	94 600
3D	704	719	0.1	13	89 600
	704	/1/	0.1	13	
A 1 0.8	2A/3A	1000 	B 600 500 400	2A/3A	1000 1300 1400 1500
0.6 Abs (a.u.)	500	1700 — 1800 — 2000	100 100 45	50 550	1700 1800 2000
	Wavelength (nm)		43		ength (nm)
C 0.5 0.4 (7 0.3 0.3 0.2 0.1 0.1 0.400	2B/3B 500 600 Wavelength (nn		D 160 140 120 n 100 e. 80 40 20 0 64	0 690	28/38 1800 1900 2000 2200 2740 790 agth (nm)
0.8 0.6 ('n'e') 0.4 0.2 0.2 0.4 50	2C/3C 550 650 Wavelength (nn		F 600 500 300 300 200 100	650 700	C/3C100 150 200 250 300 750 800
G 1 0.8 0.6 0.4 0.2 0.2 0.4 0.0 400	2D/3D 600 Wavelength (nm		H 250 200 3 150 6 100 50	2D/3D 2D/3D 700 Wavelet	

Figure 2. Analysis of the titration of different equivalents of TFA with probes **2A–2D** to form **3A–3D** in CHCl₃. Absorption spectra (A, C, E, G) and emission spectra (B, D, F, H).

for probe 3B was 86 nm; albeit, the emission intensity is much lower than 3A (Figure 2D). Subsequently, we considered a new design strategy to prepare far-red to NIR I dyes.

In our new design strategy, the xanthene core is attached to the pyrrole and indole rings through the carbon atom (C-2) adjacent to the nitrogen (N-1).²² The dyes were prepared via the Suzuki reaction of N-Boc-pyrrole-2-boronic acid pinacol ester and N-Boc-2-indoleboronic acid with bis-triflate (1), resulting in the "rhodamine-like" 3,6-dipyrrole (2C) and 3,6diindole (2D) xanthene spirocyclic lactones (Scheme 1). When lactones 2C and 2D were treated with TFA/CHCl₃, the highly colored ring-opened chromophores 3C and 3D were formed. A proposed mechanism for the spirocyclic ringopening process with TFA is shown in Scheme 2. Upon opening the lactone rings to the chromophores 3C and 3D, the absorption maxima were determined to be 665 and 704 nm, respectively, while the emission wavelengths were 717 and 719 nm, respectively. Both dyes had photophysical properties in the far-red to NIR I region with Stokes shifts of 52 and 13 nm, respectively. The reason for the lack of a trend in the Stokes shift for the dyes is currently unknown and is under investigation. Remarkably, the pyrrole derivative 3C and the indole derivative 3D had a 112 and 151 nm bathochromic shift in the absorption spectra compared to rhodamine B.

The photophysical properties of the dyes were studied in several solvents (Figure S1). All of the probes were soluble in chloroform and acetonitrile, but only the pyrrole series (3A and 3C) were soluble in 10% DMSO:water and only 3C was soluble in ethanol. The dyes had the optimal photophysical properties in CHCl₃, exhibiting moderate to large molar extinction coefficients (ε) in the range of 38 000–95 000 (M⁻¹ cm⁻¹), with the pyrrole series having a higher ε than the indole series (Table 1). It is worth noting that the emissions of the indole series were extremely weak in other solvents besides chloroform and therefore the spectra were not obtained. Probes 3C and 3D showed the best response in the NIR I region; consequently, their quantum yields were determined to be 6 and 0.1%, respectively. While the absorption maxima and molar absorptivity (ε) of the indole derivative (3D) were comparable to the pyrrole derivative (3C) in CHCl₃, its emission intensities were much lower for the same concentration. Subsequently, probe 3C was chosen for the fluoride ion detection studies.

The absorption and emission maxima for all of the probes were determined from titration with TFA in CHCl₃, with the measurements taken 10 min after mixing (Figure 2A–H). While the absorbance intensity increased with increasing concentration of TFA for all of the probes as expected, the emission response was different. The emission intensity increased for the pyrrole series (3A and 3C) with increasing concentration of TFA; on the other hand, the emission

Scheme 2. Proposed Ring-Opening Mechanism for Spirolactone Probe 2C under Acidic Conditions

intensity decreased with increasing concentration of TFA for the indole series (3B and 3D) after the initial opening of the probes. The reason for the emission response of the indole series is currently unknown and will be investigated. Interestingly, a very large number of equivalents of TFA (>100 equiv) was required to open the spirolactone rings in CHCl₃, indicating slow reaction kinetics (large activation barrier, E_a) for the ring-opening process in this solvent. This large E_a could be a result of a late transition state (TS) where the TS structure resembles the product, which is a charged compound, as postulated by the Hammond principle. We performed the measurements in ethanol (EtOH), which is a more polar solvent that can stabilize the late transition state structure more than CHCl3. A much lower number of equivalents of TFA (12 equiv) was able to open the spirolactone ring for 2C in EtOH (Figure S2). Unfortunately, all of the other probes were either insoluble or partially soluble in EtOH, and the measurements with TFA were not performed. Consequently, a time-dependent study in CHCl₃ was performed on dyes 2A and 2C (Figure S3). The timedependent study was performed with the lowest equivalent of TFA needed to open the dye: 1300 and 100 equivalents for 2A and 2C, respectively. It was seen that the dye continued to react with TFA up to 24 h, although no additional TFA was introduced to the system, which is consistent with slow kinetics. There is a bathochromic shift in the emission maxima for probe 3A after 1600 equivalents of TFA, which correlates with a change in the shape of the absorption spectrum. The absorption spectrum showed two peaks at the maximum wavelength in which the peak at the longer wavelength (531 nm) increased much faster than the peak at the shorter wavelength (477 nm). Furthermore, the peaks merged in the absorption spectrum at the same concentration that the shift occurred in the emission spectrum. The reason for the changes in these spectra in unknown; however, it is speculated that this phenomenon is due to a subtle change in the ground state structure of the probe that occurred at a much lesser extent in the other dyes. This structural change was investigated by ¹H NMR. Furthermore, a 10-fold increase in the number of equivalents of TFA was needed to open probes 2A and 2B compared to probes 2C and 2D. This difference in the TFA equivalents for opening the probes is likely due to the difference in the E_a of the dyes (2A and 2B versus 2C and 2D), which would also be related to a late TS structure. To query this phenomenon, DFT calculations were performed to determine the energy difference for the closed and opened states of 2A and 3A versus 2C and 3C (Figure S4). The experiment was done by calculating the ground state energy difference between the closed states (2A versus 2C) and the opened states (3A versus 3C). It was shown that the energy to go from 2C to 3C was 6.40 kcal/mol lower than the energy to go from 2A to 3A. Thus, assuming that the system with the lower enthalpy (2C/3C) also has the lower E_a due to the similarities in their structures, a lower equivalent of TFA would be needed to open the ring of 2C compared to 2A.

¹H NMR spectroscopy was performed to verify the structural integrity and efficacy of the probes during their response to pH in CHCl₃ (Figure S5). The ¹H NMR results show a general downfield shifting of the protons on the xanthene ring as well as the protons closest to the nitrogen atoms on the pyrrole rings for **2A** and **2C**. Since there was only one set of peaks for each proton, it is assumed that the equilibration between the ring-opened and -closed forms of the

probes is fast on the NMR time scale. Furthermore, 2A required upward of 15 equivalents of TFA for the complete opening of the spirocyclic ring, while 2C only required 5 equivalents of TFA to reach the same state. No further change occurred in the ¹H NMR spectra upon an additional increase in the TFA concentration. This result confirms that the structural integrities of the probes were maintained and verifies the need for a higher concentration of TFA to completely open probe 2A versus 2C. While there was no evidence of structural changes in the ¹H NMR with a large excess of TFA for probe 2A as speculated in the UV data, the structural changes that lead to ground state changes in the absorption spectrum could be very small or could not be deduced by ¹H NMR; thus, more studies are needed to make a definite conclusion about the absorption and emission data for 2A. It should be noted that a lower equivalent of TFA was used to open the probes in the ¹H NMR experiment compared to the UV experiment. At low concentration of the probe such as is needed to obtain quality UV spectra, the reaction rate is very slow such that a higher concentration of TFA is needed to increase the reaction rate sufficiently to observe products after 10 min. Subsequently, an increase in the concentration of the probe, which is required to obtain quality ¹H NMR spectra, will require a lower concentration of TFA to open the lactone.

To understand the effect of the probes' structures on the absorbance maxima, we performed time-dependent density functional theory (TDDFT) calculations for the lowest excited electronic states of **3A**, **3B**, **3C**, and **3D** using the ω B97X-D functional²³ and the def2-SVPD basis set at the ω B97X-D/def2-SVPD-optimized geometries.²⁴ The attachment/detachment densities were calculated and plotted for the lowest excitation for each molecule.²⁵ The detachment density plots show the regions of space where the electron density is lost during an excitation, while the attachment density plots show the regions of space where electron increases (Figure 3A–D).

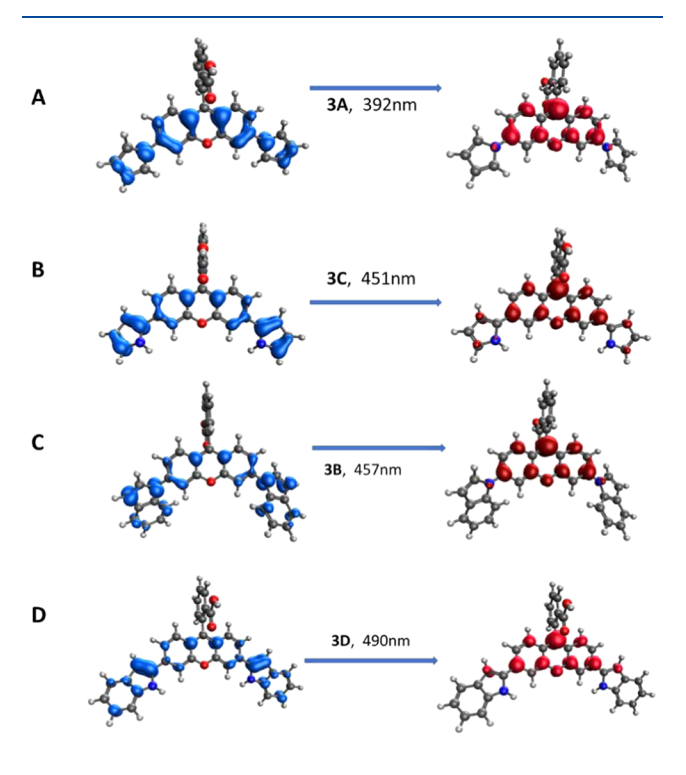


Figure 3. Attachment/detachment densities plots for probes 3A-3D.

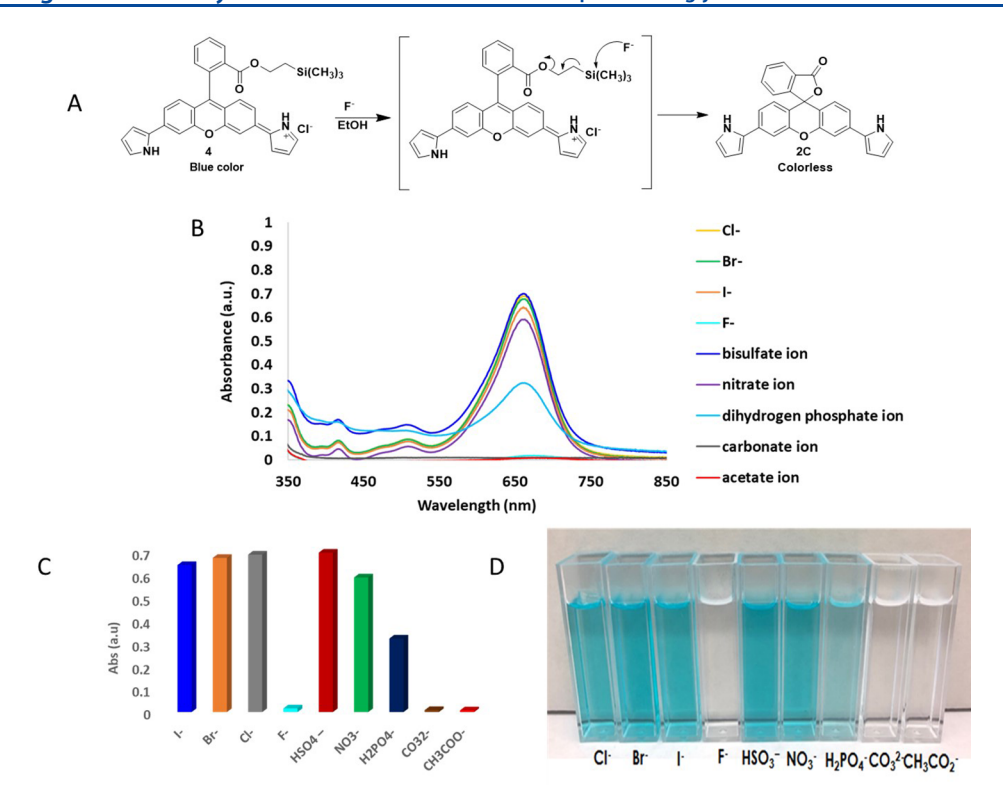


Figure 4. Response of F^- to a trimethylsilyl ethyl ester (4). Proposed mechanism for the response (A); absorption spectrum for the response of F^- (B); response to 30 equiv anions (C); and the colorimetric response of 30 equiv anions (D).

First, comparing 3A to 3B and 3C to 3D shows that the inclusion of the indole rings leads to substantially longer-wavelength excitations than is present with the pyrrole rings. Additionally, the detachment densities show more delocalization with the indole derivatives, which leads to a lower-energy excitation. Second, attaching the xanthene core through the C-2 atom leads to a significant red shift relative to attaching the rings through the N-1 atom (3A versus 3C and 3B versus 3D). Conjugation through the N-1 atom appears to block the attachment densities from containing contributions from the pyrrole and indole rings, thus reducing the delocalization of the excited states and hence increasing their energies.

To demonstrate the applicability of the dyes to detect fluoride ions, we developed a fluoride ion colorimetric probe based on 3C since it was the most soluble of the dyes. The dye was esterified with a trimethylsilyl (TMS) ethyl group to prepare the open and colored form (compound 4) (Figure S6). The silyl ester derivative 4 was soluble in all of the solvents tested with absorption maxima between 650 and 680 nm (Figure S7). The quantum yield for compound 4 was measured to be 5%, which is similar to probe 3C. The probe was treated with fluoride ions in ethanol and the measurements were taken after 10 min. It is proposed that the silylethyl group can be removed with fluoride ions resulting in the probe closing to the colorless spirocyclic form (Figure 4A). The probe responded to fluoride ions in ethanol at low concentration (Figure 4B), which corroborates the result for its response to TFA in ethanol. This design makes for a very good turn-off sensor. Additionally, the probe was tested against other anions such as halides, carbonate, phosphate, nitrate, sulfate, and acetate and shown to respond strongly to the carbonate and acetate and weakly to phosphate (Figure 4B,C). It is our belief that the response to acetate, carbonate, and

phosphate is due to the susceptibility of the TMS group to basic conditions. It has been shown in the literature that the *t*-butyldimethylsilyl (TBDMS) group does not react with acetate or phosphate ions, ²⁶ while in some cases, these ions were not tested. ²⁷ To our knowledge, there has been no report with carbonate ions. The photostability of the probe in different solvents was measured by UV/vis. ^{5c} There was no difference in the response of the probe to light versus the dark in all of the solvents tested, suggesting photostability of the probe to visible light for 80 min (Figure 5). While the probe was stable to light for 80 min, it was not stable in all of the solvents. For example, compound 4 maintained its stability in CHCl₃, acetone, and CH₃CN; however, there was a decrease in the absorbance intensity in DMSO, EtOH, and 10% of those solvents in water in the dark over the 80 min period (Figure S8). Since our

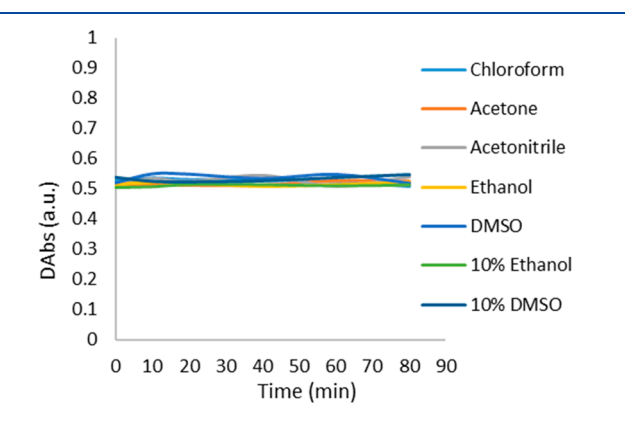


Figure 5. Response of the trimethylsilyl ester derivative of probe 3C to visible light in the presence of various solvents. ΔAbs —the difference between abs in the dark and the light.

measurements are taken within 10 min in EtOH, we do not attribute the probe's response to fluoride ions to its instability in EtOH.

The limit of detection (LOD) of the silyl ester probe for F-was calculated using absorption analysis according to the following equation: Detection limit = $3\sigma/k$, where σ is the standard deviation of blank solution with silyl ester probe and k is the slope of the calibration plot. The absorption intensity of the probe without the F- was measured 10 times and the standard deviation of the blank measurement was obtained. The slope was obtained using a plot of absorption intensity of the probe versus the concentration of F-, as shown in Figure S9. The slope and the LOD were calculated to be k = 0.0005 and 13.28 μ M (706 μ g/L), respectively. It should be noted that the LOD of F- in drinking water is 1500 μ g/L, which is 2 times higher than the LOD for our probe.

In conclusion, we have developed a new strategy to obtain far-red to NIR I xanthene-based dyes that do not require lengthy synthetic steps. In our design strategy, we combine the electron-deficient xanthene core with electron-rich pyrrole and indole; albeit, the connections are through the C-2 atoms and not through the N-1 atoms as are common for rhodamine dyes. The dyes were prepared in two steps from fluorescein and had absorption and emission maxima between 650 and 715 nm, which are in the far-red to NIR I region. Particularly, probe 3C was the most efficient dye as it had absorption and emission maxima at 665 and 717 nm, respectively, with a Stokes shift around 50 nm and a 6% quantum yield. Moreover, 3C was shown to be photostable in CHCl₃, CH₃CN, and acetone and could be used to design an efficient turn-off colorimetric probe, such as fluoride ions.

■ EXPERIMENTAL SECTION

All reactions were performed under an inert atmosphere, utilizing glassware that were flame-dried and cooled under vacuum. Reactions were monitored using thin-layer chromatography (TLC) on silica gel plates and ¹H NMR. Unless otherwise indicated, all starting materials, catalysts, and ligands were obtained from Sigma-Aldrich, Oakwood, or Fisher and used without further purification.

¹H NMR and ¹³C NMR spectra were recorded in deuterated solvents on a Bruker AVANCE 300, 500, and 600 Hz NMR Spectrometer. *J* values are expressed in Hz and quoted chemical shifts are in ppm downfield from tetramethylsilane (TMS) reference using the residual protonated solvents as an internal standard. The signals have been designated as follows: s (singlet), d (doublet), t (triplet), and m (multiplets). The melting point was measured on a la Venta MEL-TEMP 1101D melting point apparatus. The samples were finely grinded and filled into a capillary tube for measurement. High-resolution mass spectra (HRMS) were determined on a Bruker-micrOTOF-Q II Mass Spectrometer. Absorption spectra were acquired using a Cary 60 UV–Vis instrument and fluorescence analysis was done using a Cary Eclipse Fluorescence Spectrophotometer.

UV/FI Analysis. Analysis for the Ring Opening of Each Probe Using Different Equivalents of TFA. Four milliliters of a 100 μ M solution of each probe in chloroform was prepared and different equivalents of TFA were added. The solutions were allowed to sit for 10 min before taking the measurements. The analysis was repeated for probe 2C in ethanol.

Determination of Molar Absorptivity Coefficient Values. For each probe (2A, 2B, 2C, 2D), a 1.0 mM stock solution was prepared in different solvents (chloroform, acetonitrile, EtOH, and 10% DMSO/ $\rm H_2O$) from which different concentrations of the probe were made and used for analysis. To each concentration, excess TFA was added to ensure complete ring opening and the UV and FI measurements were taken after 10 min. The Beer–Lambert law was

used to calculate the molar absorptivity coefficient values for all of the probes in different solvents.

NMR Study with TFA. Solutions (1.0 mM) of probes 2A and 2C in CD₂Cl₂ were prepared to which different equivalents of deuterated TFA were added. ¹H NMR analysis was obtained after 10 min.

Quantum Yield. Solution absolute photoluminescence quantum yields were determined with a Quantaurus-QY C11347 spectrometer in $\mathrm{CHCl_3}$ solution with absorbance less than 0.1. Probe 3C was excited at 650 nm, 3D was excited at 690 nm, and 4 was excited at 650 nm.

Analysis of Compound 4 with Different Equivalents of Fluoride Ion. A 500 μ M stock solution of probe 4 was prepared by dissolving 1.33 mg of the probe in 5 mL of ethanol. A 30 μ M solution was prepared from the stock solution by taking 300 μ L in 5 mL ethanol. For the fluoride source, a 100 mM KF stock solution (in de-ionized (DI) water) was prepared and used accordingly. To the 30 μ M solution of probe 4 were added different equivalents of KF solution and the UV—vis spectrum was recorded after 10 min.

Anion Selectivity Measurements. Thirty equivalents of a 100 mM aqueous solution of each ion (Cl⁻, Br⁻, I⁻, HSO₄⁻, NO₃⁻, H₂PO₄⁻, CH₃COO⁻, and CO₃²⁻) was added to 5 mL of a 30 μ M solution of probe 4 in ethanol and the UV–vis spectrum was recorded after 10 min

Synthesis of Probes. Probes **2A** and **2B** were prepared according to the literature procedures, ²⁰ while **2C** and **2D** were synthesized by modifying the previously reported procedure.³⁰

3',6'-Di(1H-pyrrol-2-yl)-3H-spiro[isobenzofuran-1,9'-xanthen]-3one (2C). Fluorescein ditriflate (0.168 mmol, 100 mg), N-Bocpyrrole-2-boronic acid pinacol ester (0.503 mmol, 147.6 mg), 6 equiv of KOAC (1.006 mmol, 98.8 mg), and 6 mol % of Pd(PPh₃)₄ (0.0101 mmol, 11.6 mg) were added into a flamed-dried microwave reaction vial in a glovebox under a nitrogen atmosphere. The tube was sealed and removed from the glovebox to which 3 mL of 1,4-dioxane:water (2:1) was added and the reaction mixture was heated at 100 °C in an oil bath for 24 h. The reaction was monitored by TLC and ¹H NMR. The reaction mixture was allowed to come to room temperature, followed by the addition of water (25 mL) and extracted with CH₂Cl₂ $(3 \times 20 \text{ mL})$. The combined organic layer was dried over anhydrous Na₂SO₄, filtered, and concentrated under vacuum. The crude product was purified by column chromatography on silica gel with a hexane:ethyl acetate (70:30) mixture to give the product (2C) as a blue-colored solid in 80% yield. mp 172-180 °C. ¹H NMR (500 MHz, CD_2Cl_2) δ 8.88 (s, 2H), 8.05 (d, J = 7.3 Hz, 1H), 7.71–7.59 (m, 2H), 7.30 (s, 2H), 7.13 (dd, J = 13.7, 7.9 Hz, 3H), 6.89 (s, 2H),6.74 (d, J = 8.3 Hz, 2H), 6.58 (s, 2H), 6.30 (d, J = 1.9 Hz, 2H). $^{13}C\{^{1}H\}$ NMR (126 MHz, $CD_{2}Cl_{2}$) δ 170.0, 153.4, 151.9, 135.6, 135.55, 130.54, 130.2, 128.6, 126.5, 125.3, 124.1, 120.3, 119.5, 116.2, 111.5, 110.4, 107.7, 83.1. HRMS (ESI) m/z: $[M + H]^+$ calcd for C₂₈H₁₈N₂O₃H; 431.1390, found 431.1373.

3',6'-Di(1H-indol-2-yl)-3H-spiro[isobenzofuran-1,9'-xanthen]-3one (2D). Fluorescein ditriflate (0.168 mmol, 100 mg), N-Bocpyrrole-2-boronic acid pinacol ester (0.503 mmol, 131.3 mg), 6 equiv of KOAC (1.01 mmol, 98.8 mg), and 6 mol % of Pd(PPh₃)₄ (0.0101 mmol, 11.6 mg) were added into a flamed-dried microwave reaction vial in a glovebox under nitrogen atmosphere. The tube was sealed and removed from the glovebox to which 3 mL of 1,4-dioxane:water (2:1) was added and the reaction mixture was heated at 100 °C in an oil bath for 48 h. The reaction was monitored by TLC and ¹H NMR. The reaction mixture was allowed to come to room temperature, followed by the addition of water (25 mL), and extracted with CH_2Cl_2 (3 × 20 mL). The combined organic layer was dried over anhydrous Na₂SO₄, filtered, and concentrated under vacuum. The crude product was purified by column chromatography on silica gel with a hexane:ethyl acetate (70:30) mixture to give the product (2D) as a yellowish white solid in 85% yield. mp 240-245 °C. ¹H NMR (500 MHz, acetone) δ 10.81 (s, 2H), 8.08 (d, J = 7.5 Hz, 1H), 7.87 (s, 2H), 7.80 (dt, J = 23.3, 7.4 Hz, 2H), 7.63 (dd, J = 8.3, 1.4 Hz, 2H), 7.60 (d, J = 7.9 Hz, 2H), 7.45 (d, J = 8.1 Hz, 2H), 7.38 (d, J = 7.6 Hz, 2Hz, 2Hz)1H), 7.16 (t, J = 7.6 Hz, 2H), 7.08-7.03 (m, 4H), 6.97 (d, J = 8.3 Hz, 2H). $^{13}\text{C}\{^1\text{H}\}$ NMR (126 MHz, acetone) δ 169.5, 153.9, 152.5,

138.6, 137.1, 136.4, 136.3, 131.1, 130.0, 129.6, 127.2, 125.7, 124.9, 123.4, 121.8, 121.5, 120.8, 118.7, 113.7, 112.2, 101.7, 82.5. HRMS (ESI) m/z: [M + H]⁺ calcd for $C_{36}H_{22}N_2O_3H$; 531.1703, found 531.1703.

General Synthesis of 3A–3D. To a CHCl₃ solution of **2A–2D** was added the minimum amount of a TFA in CHCl₃ solution (5–20 equiv) that would allow the dyes to be fully converted to the opened form when allowed to stir at rt for 10 min. Analysis was taken of this solution. Note: for ¹H and ¹³C NMR analyses, the solutions were made in deuterated solvents.

1-[9-(2-Carboxyphenyl)-6-(1H-pyrrol-1-yl)-3H-xanthen-3-ylidene]-1H-1lambda5-pyrrol-1-ylium (3A). 1 H NMR (600 MHz, CD₂Cl₂) δ 8.46 (d, J = 7.9 Hz, 1H), 7.95 (dt, J = 30.0, 7.6 Hz, 2H), 7.89 (s, 1H), 7.69 (d, J = 9.1 Hz, 2H), 7.55 (d, J = 9.1 Hz, 2H), 7.43 (d, J = 7.5 Hz, 1H), 7.39 (s, 4H), 6.55 (s, 4H). 13 C{ 1 H} NMR (151 MHz, CD₂Cl₂) δ 159.1, 151.5, 135.4, 133.9, 133.3, 133.2, 132.7, 130.4, 120.9, 120.5, 120.2, 118.2 116.5, 114.4, 112.5, 105.9. HRMS (ESI) m/z: [M]⁺ calcd for C₂₈H₁₉N₂O₃⁺ 431.1390; found 431.1394.

1-[(3E)-9-(2-Carboxyphenyl)-6-(1H-indol-1-yl)-3H-xanthen-3-ylidene]-1H-1lambda5-indol-1-ylium (**3B**). ¹H NMR (500 MHz, CD₂Cl₂) δ 8.60 (d, J = 7.9 Hz, 1H), 8.27 (s, 2H), 8.16-7.90 (m, 6H), 7.76 (d, J = 8.5 Hz, 4H), 7.63 (s, 2H), 7.54 (d, J = 7.5 Hz, 1H), 7.46 (t, J = 7.7 Hz, 2H), 7.39 (t, J = 7.4 Hz, 2H), 7.00 (s, 2H). ¹³C{¹H} NMR (151 MHz, CD₂Cl₂) δ 159.0, 152.0 135.8, 135.6, 133.8, 133.5, 133.1, 132.8, 132.4, 130.6, 127.3, 125.6, 124.8, 123.8, 123.2, 120.9, 118.0, 116.1, 114.2, 112.6, 112.3, 111.8, 108.9. HRMS (ESI) m/z: [M]⁺ calcd for C₃₆H₂₃N₂O₃⁺ 531.1703; found 531.1727.

2-[(3E)-9-(2-Carboxyphenyl)-6-(1H-pyrrol-2-yl)-3H-xanthen-3-ylidene]-2H-pyrrol-1-ium (3C). ¹H NMR (500 MHz, CD₂Cl₂) δ 8.52 (d, J = 7.8 Hz, 1H), 7.95 (dd, J = 22.4, 7.5 Hz, 2H), 7.89 (s, 2H), 7.75 (d, J = 8.8 Hz, 2H), 7.43 (d, J = 7.4 Hz, 1H), 7.38 (d, J = 8.8 Hz, 2H), 7.26 (s, 2H), 7.14 (s, 2H), 6.48 (s, 2H). ¹³C{¹H} NMR (151 MHz, CD₂Cl₂) δ 170.5, 165.1, 158.4, 145.3, 135.3, 134.1, 133.3, 132.1, 131.7–130.2, 128.7, 125.3, 121.8, 118.0, 116.1, 114.2, 112.4, 109.1. HRMS (ESI) m/z: [M]⁺ calcd for C₂₈H₁₉N₂O₃⁺ 431.1390; found 431.1390.

1-[(3E)-9-(2-Carboxyphenyl)-6-(1H-indol-1-yl)-3H-xanthen-3-ylidene]-1H-1lambda5-indol-1-ylium (3D).
¹H NMR (500 MHz, CD₂Cl₂) δ 8.59 (d, J = 7.9 Hz, 1H), 8.20 (s, 2H), 8.08–7.94 (m, 5H), 7.71 (d, J = 8.1 Hz, 2H), 7.55 (d, J = 8.8 Hz, 2H), 7.49 (dd, J = 14.7, 8.6 Hz, 3H), 7.39 (t, J = 7.6 Hz, 2H), 7.19 (t, J = 7.6 Hz, 2H).
¹³C{¹H} NMR (126 MHz, CD₂Cl₂) δ 178.0, 167.4, 158.8, 146.2, 140.8 (s), 135.7, 135.0, 134.1, 133.7, 132.7, 131.1, 131.1, 129.7, 128.2, 127.1, 123.4, 123.3, 122.8, 118.6, 116.4, 114.1, 112.9, 111.9, 111.8. HRMS (ESI) m/z: [M]⁺ calcd for C₃₆H₂₃N₂O₃⁺ 531.1703; found 531.1725.

Synthesis of Trimethylsilyl Ester Derivative (4). The compound was prepared following modification of a previously reported procedure. 22 To a solution of 2C (50 mg, 0.116 mmol) in 2 mL of dry 1,2-dichloroethane (DCE) under a nitrogen atmosphere was added dropwise phosphorous oxychloride (0.03 mL, 3 equiv). The resulted blue-colored solution was refluxed in an oil bath for 4 h. The reaction mixture was cooled and concentrated under reduced pressure to give the acid chloride product, which was used in the next step without further purification. To the crude acid chloride was added excess 2-trimethylsilylethanol (2 mL) and the reaction mixture was stirred at 50 °C in an oil bath for 24 h. Excess 2trimethylsilylethanol was removed under reduced pressure and the blue-colored residue was dissolved in chloroform (20 mL) and washed with distilled water (3 × 25 mL). The organic layer was dried over anhydrous Na2SO4 and concentrated under reduced pressure. The residue was sonicated and washed with hexane several times (15-20) to remove all nonpolar impurities before being subjected to column chromatography on silica gel with CHCl3:MeOH (10:1) to give the product as a blue solid, which was precipitated from ethyl acetate, dried under reduced pressure to give the purified product as a blue solid in 45% yield. ¹H NMR (300 MHz, CD_2Cl_2) δ 12.76 (s, 2H), 8.39 (d, J = 7.6 Hz, 1H), 8.07 (d, J = 7.9 Hz, 2H), 7.88 (td, J =15.2, 7.0 Hz, 4H), 7.41 (d, J = 7.4 Hz, 1H), 7.32 (d, J = 9.0 Hz, 2H), 7.02 (s, 2H), 6.84 (s, 2H), 6.16 (s, 2H), 4.09-4.01 (t, 2H), 0.820.59 (t, 2H), -0.09 (s, 9H). 13 C{ 1 H} NMR (126 MHz, CD₂Cl₂) δ 165.4, 157.7, 145.1 133.8, 133.5, 131.8, 131.3, 131.1, 130.5, 130.3, 128.9, 125.3, 121.5, 115.7, 112.9, 110.3, 64.7, 17.5, -1.4. HRMS (ESI) [M] $^{+}$ calcd for C₃₃H₃₁N₂O₃Si $^{+}$ 531.2098; found 531.2098.

ASSOCIATED CONTENT

Supporting Information

The Supporting Information is available free of charge at https://pubs.acs.org/doi/10.1021/acs.joc.0c01242.

Absorption spectra for solvents effects, response to TFA in EtOH, photostability, etc.; DFT calculations for energy differences 2A/3A versus 2C/3C; proton and carbon NMR (PDF)

AUTHOR INFORMATION

Corresponding Authors

Seth Marder — School of Chemistry and Biochemistry, Georgia Institute of Technology, Atlanta, Georgia 30332-0400, United States; Occid.org/0000-0001-6921-2536;

Email: seth.marder@chemistry.gatech.edu

Steven R. Gwaltney — Department of Chemistry, Mississippi State University, Mississippi State, Mississippi 39762, United States; Email: sgwaltney@chemistry.msstate.edu

Colleen N. Scott — Department of Chemistry, Mississippi State University, Mississippi State, Mississippi 39762, United States; orcid.org/0000-0003-3332-2439; Email: cscott@chemistry.msstate.edu

Authors

Ishanka Rajapaksha — Department of Chemistry, Mississippi State University, Mississippi State, Mississippi 39762, United States

Hao Chang – Department of Chemistry, Mississippi State
 University, Mississippi State, Mississippi 39762, United States
 Yao Xiong – School of Chemistry and Biochemistry, Georgia
 Institute of Technology, Atlanta, Georgia 30332-0400, United
 States

Complete contact information is available at: https://pubs.acs.org/10.1021/acs.joc.0c01242

Notes

The authors declare no competing financial interest.

ACKNOWLEDGMENTS

We are grateful for the financial support from the National Science Foundation for award OIA-1757220.

REFERENCES

(1) (a) Armin, A.; Jansen-van Vuuren, R. D.; Kopidakis, N.; Burn, P. L.; Meredith, P. Narrowband light detection via internal quantum efficiency manipulation of organic photodiodes. *Nat. Commun.* 2015, 6, No. 6343. (b) García de Arquer, F. P.; Armin, A.; Meredith, P.; Sargent, E. H. Solution-processed semiconductors for next-generation photodetectors. *Nat. Rev. Mater.* 2017, 2, No. 16100. (c) Siegmund, B.; Mischok, A.; Benduhn, J.; Zeika, O.; Ullbrich, S.; Nehm, F.; Böhm, M.; Spoltore, D.; Fröb, H.; Körner, C.; Leo, K.; Vandewal, K. Organic narrowband near-infrared photodetectors based on intermolecular charge-transfer absorption. *Nat. Commun.* 2017, 8, No. 15421. (d) Liu, X.; Lin, Y.; Liao, Y.; Wu, J.; Zheng, Y. Recent advances in organic near-infrared photodiodes. *J. Mater. Chem. C* 2018, 6, 3499–3513.

(2) (a) Zhang, M.; Jin, R. Rational design of near-infrared dyes based on boron dipyrromethene derivatives for application in organic solar cells. *RSC Adv.* **2018**, *8*, 33659–33665. (b) Bürckstümmer, H.;

- Kronenberg, N. M.; Meerholz, K.; Würthner, F. Near-infrared absorbing merocyanine dyes for bulk heterojunction solar cells. *Org. Lett.* **2010**, *12*, 3666–3669.
- (3) (a) Li, W.; Liu, Z.; Xu, X.; Cheng, Y.-B.; Zhao, Z.; He, H. Near-infrared absorbing porphyrin dyes with perpendicularly extended π-conjugation for dye-sensitized solar cells. *RSC Adv.* **2014**, *4*, 50897–50905. (b) Kolemen, S.; Cakmak, Y.; Erten-Ela, S.; Altay, Y.; Brendel, J.; Thelakkat, M.; Akkaya, E. U. Solid-State Dye-Sensitized Solar Cells Using Red and Near-IR Absorbing Bodipy Sensitizers. *Org. Lett.* **2010**, *12*, 3812–3815.
- (4) (a) Allen, C. M.; Sharman, W. M.; Van Lier, J. E. Current status of phthalocyanines in the photodynamic therapy of cancer. *J. Porphyrins Phthalocyanines* **2001**, *05*, 161–169. (b) Sharman, W. M.; Allen, C. M.; van Lier, J. E. Photodynamic therapeutics: basic principles and clinical applications. *Drug Discovery Today* **1999**, *4*, 507–517. (c) Detty, M. R.; Gibson, S. L.; Wagner, S. J. Current Clinical and Preclinical Photosensitizers for Use in Photodynamic Therapy. *J. Med. Chem.* **2004**, *47*, 3897–3915.
- (5) (a) Fabian, J.; Nakazumi, H.; Matsuoka, M. Near-infrared absorbing dyes. Chem. Rev. 1992, 92, 1197–1226. (b) Matsuoka, M. Infrared Absorbing Dyes; Plenum Press: New York, 1990. (c) Weissleder, R. A clearer vision for in vivo imaging. Nat. Biotechnol. 2001, 19, 316–317. (d) Grzybowski, M.; Taki, M.; Senda, K.; Sato, Y.; Ariyoshi, T.; Okada, Y.; Kawakami, R.; Imamura, T.; Yamaguchi, S. A Highly Photostable Near-Infrared Labeling Agent Based on a Phospha-rhodamine for Long-Term and Deep Imaging. Angew. Chem., Int. Ed. 2018, 57, 10137–10141. (e) Niu, G.; Liu, W.; Zhou, B.; Xiao, H.; Zhang, H.; Wu, J.; Ge, J.; Wang, P. Deep-Red and Near-Infrared Xanthene Dyes for Rapid Live Cell Imaging. J. Org. Chem. 2016, 81, 7393–7399.
- (6) (a) Hu, L.; Yan, Z.; Xu, H. Advances in synthesis and application of near-infrared absorbing squaraine dyes. RSC Adv. 2013, 3, 7667–7676. (b) Qin, C.; Wong, W.-Y.; Han, L. Squaraine Dyes for Dye-Sensitized Solar Cells: Recent Advances and Future Challenges. Chem. Asian J. 2013, 8, 1706–1719. (c) Umezawa, K.; Citterio, D.; Suzuki, K. Water-soluble NIR Fluorescent Probes Based on Squaraine and Their Application for Protein Labeling. Anal. Sci. 2008, 24, 213–217. (d) Lambert, C.; Scherpf, T.; Ceymann, H.; Schmiedel, A.; Holzapfel, M. Coupled Oscillators for Tuning Fluorescence Properties of Squaraine Dyes. J. Am. Chem. Soc. 2015, 137, 3547–3557.
- (7) (a) Brogdon, P.; Cheema, H.; Delcamp, J. H. Near-Infrared-Absorbing Metal-Free Organic, Porphyrin, and Phthalocyanine Sensitizers for Panchromatic Dye-Sensitized Solar Cells. *ChemSusChem* 2018, 11, 86–103. (b) Braun, A. B.; Wehl, I.; Kölmel, D. K.; Schepers, U.; Bräse, S. New Polyfluorinated Cyanine Dyes for Selective NIR Staining of Mitochondria. *Chem. Eur. J.* 2019, 25, 7998–8002. (c) Gayton, J.; Autry, S. A.; Meador, W.; Parkin, S. R.; Hill, G. A.; Hammer, N. I.; Delcamp, J. H. Indolizine-Cyanine Dyes: Near Infrared Emissive Cyanine Dyes with Increased Stokes Shifts. *J. Org. Chem.* 2019, 84, 687–697.
- (8) (a) Kuimova, M. K.; Collins, H. A.; Balaz, M.; Dahlstedt, E.; Levitt, J. A.; Sergent, N.; Suhling, K.; Drobizhev, M.; Makarov, N. S.; Rebane, A.; Anderson, H. L.; Phillips, D. Photophysical properties and intracellular imaging of water-soluble porphyrin dimers for two-photon excited photodynamic therapy. *Org. Biomol. Chem.* **2009**, *7*, 889–896. (b) Nesterova, I. V.; Verdree, V. T.; Pakhomov, S.; Strickler, K. L.; Allen, M. W.; Hammer, R. P.; Soper, S. A. Metallo-phthalocyanine near-IR fluorophores: oligonucleotide conjugates and their applications in PCR assays. *Bioconjugate Chem.* **2007**, *18*, 2159–2168.
- (9) (a) Lu, H.; Mack, J.; Yang, Y.; Shen, Z. Structural modification strategies for the rational design of red/NIR region BODIPYs. *Chem. Soc. Rev.* **2014**, 43, 4778–4823. (b) Staudinger, C.; Breininger, J.; Klimant, I.; Borisov, S. M. Near-infrared fluorescent aza-BODIPY dyes for sensing and imaging of pH from the neutral to highly alkaline range. *Analyst* **2019**, 144, 2393–2402.
- (10) Grzybowski, M.; Gryko, D. T. Diketopyrrolopyrroles: Synthesis, Reactivity, and Optical Properties. *Adv. Opt. Mater.* **2015**, *3*, 280–320.

- (11) (a) Sibrian-Vazquez, M.; Escobedo, J. O.; Lowry, M.; Fronczek, F. R.; Strongin, R. M. Field Effects Induce Bathochromic Shifts in Xanthene Dyes. J. Am. Chem. Soc. 2012, 134, 10502–10508. (b) Wang, L. G.; Munhenzva, I.; Sibrian-Vazquez, M.; Escobedo, J. O.; Kitts, C. H.; Fronczek, F. R.; Strongin, R. M. Altering Fundamental Trends in the Emission of Xanthene Dyes. J. Org. Chem. 2019, 84, 2585–2595. (c) Sun, Y.-Q.; Liu, J.; Lv, X.; Liu, Y.; Zhao, Y.; Guo, W. Rhodamine-Inspired Far-Red to Near-Infrared Dyes and Their Application as Fluorescence Probes. Angew. Chem., Int. Ed. 2012, 51, 7634–7636. (d) Myochin, T.; Hanaoka, K.; Komatsu, T.; Terai, T.; Nagano, T. Design Strategy for a Near-Infrared Fluorescence Probe for Matrix Metalloproteinase Utilizing Highly Cell Permeable Boron Dipyrromethene. J. Am. Chem. Soc. 2012, 134, 13730–13737.
- (12) (a) Niu, G.; Liu, W.; Zhou, B.; Xiao, H.; Zhang, H.; Wu, J.; Ge, J.; Wang, P. Deep-Red and Near-Infrared Xanthene Dyes for Rapid Live Cell Imaging. J. Org. Chem. 2016, 81, 7393–7399. (b) Liu, J. X.; Diwu, Z. J.; Leung, W. Y.; Lu, Y.; Patcha, B.; Hauglanda, R. P. Rational design and synthesis of a novel class of highly fluorescent rhodamine dyes that have strong absorption at long wavelengths. Tetrahedron Lett. 2003, 44, 4355–4359. (c) Kubin, R. F.; Fletcher, A. N. Fluorescence quantum yields of some rhodamine dyes. J. Lumin. 1982, 27, 455–462. (d) Rahn, M. D.; King, T. A.; Gorman, A. A.; Hamblett, I. Photostability enhancement of Pyrromethene 567 and Perylene Orange in oxygen-free liquid and solid dye lasers. Appl. Opt. 1997, 36, 5862–5871. (e) Zheng, H.; Zhan, X.-Q.; Bian, Q.-N.; Zhang, X.-J. Advances in modifying fluorescein and rhodamine fluorophores as fluorescent chemosensors. Chem. Commun. 2013, 49, 429–447.
- (13) Cui, P.; Jiang, X.; Sun, J.; Zhang, Q.; Gao, F. A water-soluble rhodamine B-derived fluorescent probe for pH monitoring and imaging in acidic regions. *Methods Appl. Fluoresc.* **2017**, *5*, No. 024009.
- (14) (a) Kim, H. N.; Lee, M. H.; Kim, H. J.; Kim, J. S.; Yoon, J. A new trend in rhodamine-based chemosensors: application of spirolactam ring-opening to sensing ions. *Chem. Soc. Rev.* **2008**, *37*, 1465–1472. (b) Valeur, B. *Molecular Fluorescence: Principles and Applications*; Wiley-VCH Verlag GmbH: New York, 2001, Chapter 10
- (15) Fu, M.; Xiao, Y.; Qian, X.; Zhao, D.; Xu, Y. A design concept of long-wavelength fluorescent analogs of rhodamine dyes: replacement of oxygen with silicon atom. *Chem. Commun.* **2008**, *15*, 1780–1782. (16) Koide, Y.; Urano, Y.; Hanaoka, K.; Terai, T.; Nagano, T. Evolution of Group 14 Rhodamines as Platforms for Near-Infrared Fluorescence Probes Utilizing Photoinduced Electron Transfer. *ACS*
- Chem. Biol. 2011, 6, 600–608. (17) (a) Egawa, T.; Koide, Y.; Hanaoka, K.; Komatsu, T.; Terai, T.; Nagano, T. Development of a fluorescein analogue, TokyoMagenta, as a novel scaffold for fluorescence probes in red region. Chem. Commun. 2011, 47, 4162–4164. (b) Best, Q. A.; Sattenapally, N.; Dyer, D. J.; Scott, C. N.; McCarroll, M. E. pH-Dependent Si-Fluorescein Hypochlorous Acid Fluorescent Probe: Spirocycle Ring-Opening and Excess Hypochlorous Acid-Induced Chlorination. J. Am. Chem. Soc. 2013, 135, 13365–13370.
- (18) (a) Fukazawa, A.; Suda, S.; Taki, M.; Yamaguchi, E.; Grzybowski, M.; Sato, Y.; Higashiyama, T.; Yamaguchi, S. Phosphafluorescein: a red-emissive fluorescein analogue with high photobleaching resistance. *Chem. Commun.* 2016, 52, 1120–1123. (b) Ogasawara, H.; Grzybowski, M.; Hosokawa, R.; Sato, Y.; Taki, M.; Yamaguchi, S. A far-red fluorescent probe based on a phosphafluorescein scaffold for cytosolic calcium imaging. *Chem. Commun.* 2018, 54, 299–302. (c) Grzybowski, M.; Taki, M.; Senda, K.; Sato, Y.; Ariyoshi, T.; Okada, Y.; Kawakami, R.; Imamura, T.; Yamaguchi, S. A Highly Photostable Near-Infrared Labeling Agent Based on a Phospha-rhodamine for Long-Term and Deep Imaging. *Angew. Chem., Int. Ed.* 2018, 57 (32), 10137–10141.
- (19) Yuan, L.; Lin, W.; Yang, Y.; Chen, H. A Unique Class of Near-Infrared Functional Fluorescent Dyes with Carboxylic-Acid-Modulated Fluorescence ON/OFF Switching: Rational Design, Synthesis,

- Optical Properties, Theoretical Calculations, and Applications for Fluorescence Imaging in Living Animals. *J. Am. Chem. Soc.* **2012**, *134*, 1200–1211.
- (20) Grimm, J. B.; Lavis, L. D. Synthesis of Rhodamines from Fluoresceins Using Pd-Catalyzed C-N Cross-Coupling. *Org. Lett.* **2011**, *13*, 6354-6357.
- (21) Woodroofe, C. C.; Lim, M. H.; Weiming, B.; Lippard, S. J. Synthesis of isomerically pure carboxylate- and sulfonate-substituted xanthene fluorophores. *Tetrahedron* **2005**, *61*, 3097–3105.
- (22) Rathnamalala, C. S. L.; Gayton, J. N.; Dorris, A. L.; Autry, S. A.; Meador, W.; Hammer, N. I.; Delcamp, J. H.; Scott, C. N. Donor–Acceptor–Donor NIR II Emissive Rhodindolizine Dye Synthesized by C–H Bond Functionalization. *J. Org. Chem.* **2019**, *84*, 13186–13193.
- (23) Chai, J.-D.; Head-Gordon, M. Long-range corrected heybrid density functionals with damped atom—atom dispersion corrections. *Phys. Chem. Chem. Phys.* **2008**, *10*, 6615–6620.
- (24) Rappoport, D.; Furche, F. Property-optimized Gaussian basis sets for molecular response calculations. *J. Chem. Phys.* **2010**, *133*, No. 134105.
- (25) Head-Gordon, M.; Grana, A. M.; Maurice, D.; White, C. A. Analysis of Electronic Transitions as the Difference of Electron Attachment and Detachment Densities. *J. Phys. Chem. A.* **1995**, *99*, 14261–14270.
- (26) (a) Zhu, C.-Q.; Chen, J.-L.; Zheng, H.; Wu, Y.-Q.; Xu, J.-G. A colorimetric method for fluoride determination in aqueous samples based on the hydroxyl deprotection reaction of a cyanine dye. *Anal. Chim. Acta* 2005, 539, 311–316. (b) Ren, J.; Wu, Z.; Zhou, Y.; Li, Y.; Xu, Z. Colorimetric fluoride sensor based on 1,8-naphthalimide derivatives. *Dyes Pigm.* 2011, 91, 442–445.
- (27) Zou, B.; Liu, H.; Mack, J.; Wang, S.; Tian, J.; Lu, H.; Li, Z.; Shen, Z. A new aza-BODIPY based NIR region colorimetric and fluorescent chemodosimeter for fluoride. *RSC Adv.* **2014**, *4*, 53864–53869.
- (28) Luo, A.; Wang, H.; Wang, Y.; Huang, Q.; Zhang, Q. A novel colorimetric and turn-on fluorescent chemosensor for iron(III) ion detection and its application to cellular imaging. *Spectrochim. Acta, Part A* **2016**, *168*, 37–44.
- (29) (a) Johnston, H. L. Rural Health Cooperatives. *Public Health Rep.* **1950**, *65*, 1383–1397. (b) Boxi, S. S.; Paria, S. Fluorometric selective detection of fluoride ions in aqueous media using Ag doped CdS/ZnS core/shell nanoparticles. *Dalton Trans.* **2016**, *45*, 811–819.
- (30) Khaddour, Z.; Akrawi, O. A.; Suleiman, A. S.; Patonay, T.; Villinger, A.; Langer, P. Regioselective Suzuki–Miyaura cross-coupling reactions of the bis(triflate) of 4,7-dihydroxycoumarin. *Tetrahedron Lett.* **2014**, *55*, 4421–4423.